THE JOURNAL OF BIOLOGICAL CHEMISTRY VOL. 286, NO. 32, pp. 28026–28040, August 12, 2011

Munc18-1 and Munc18-2 Proteins Modulate β-Cell Ca^{2+} Sensitivity and Kinetics of Insulin Exocytosis Differently*

Received for publication, February 27, 2011, and in revised form, May 30, 2011 Published, JBC Papers in Press, June 20, 2011, DOI 10.1074/jbc.M111.235366

Slavena A. Mandic[‡1], Masa Skelin[§1], Jenny U. Johansson[¶], Marjan S. Rupnik[§], Per-Olof Berggren[‡2], and Christina Bark[‡]

From [‡]The Rolf Luft Research Center for Diabetes and Endocrinology, Karolinska Institutet, 17176 Stockholm, Sweden, the [§]Institute of Physiology, Faculty of Medicine, University of Maribor, 2000 Maribor, Slovenia, and the [¶]Department of Neurology and Neurological Sciences, Stanford University, Stanford, California 94305

Fast neurotransmission and slower hormone release share the same core fusion machinery consisting of SNARE (soluble *N*-ethylmaleimide-sensitive factor attachment protein receptor) proteins. In evoked neurotransmission, interactions between SNAREs and the Munc18-1 protein, a member of the Sec1/Munc18 (SM) protein family, are essential for exocytosis, whereas other SM proteins are dispensable. To address if the exclusivity of Munc18-1 demonstrated in neuroexocytosis also applied to fast insulin secretion, we characterized the presence and function of Munc18-1 and its closest homologue Munc18-2 in β-cell stimulus-secretion coupling. We show that pancreatic β-cells express both Munc18-1 and Munc18-2. The two Munc18 homologues exhibit different subcellular localization, and only Munc18-1 redistributes in response to glucose stimulation. However, both Munc18-1 and Munc18-2 augment glucose-stimulated hormone release. Ramp-like photorelease of caged Ca^{2+} and high resolution whole-cell patch clamp recordings show that Munc18-1 and Munc18-2 overexpression shift the Ca^{2+} sensitivity of the fastest phase of insulin exocytosis differently. In addition, we reveal that Ca^{2+} sensitivity of exocytosis in β-cells depends on the phosphorylation status of the Munc18 proteins. Even though Munc18-1 emerges as the key SM-protein determining the Ca^{2+} threshold for triggering secretory activity in a stimulated β-cell, Munc18-2 has the ability to increase Ca^{2+} sensitivity and thus mediates the release of fusion-competent granules requiring a lower cytoplasmic-free Ca^{2+} concentration, $[Ca^{2+}]_i$. Hence, Munc18-1 and Munc18-2 display distinct subcellular compartmentalization and can coordinate the insulin exocytotic process differently as a consequence of the actual $[Ca^{2+}]_i$.

To maintain glucose homeostasis in the body, the pancreatic β-cell must in a controlled way produce, store, and secrete insulin in response to appropriate stimuli (1). Regulated membrane fusion resulting in insulin exocytosis in β-cells is managed by the same core SNARE[3] (soluble *N*-ethylmaleimide-sensitive factor (NSF) attachment protein receptor) fusion machinery that mediates release of chemical signals at highly specialized central neuronal synapses (2–4). Three conserved SNARE proteins, VAMP2, syntaxin 1A, and SNAP-25, connect vesicles with the plasma membrane by forming an exceptionally stable protein complex that holds the intrinsic, but slow, capability to perform lipid bilayer fusion (5). Except for the SNARE proteins, additional cooperating proteins are critical to guarantee speed and accuracy of diverse membrane fusion events occurring in excitable cells. Such a key accessory regulator in synaptic transmission is Munc18-1, a member of the Munc18 (mammalian homologue of the unc-18 gene) family (6). In addition to Munc18-1 (with two alternatively spliced variants, Munc18-1a and Munc18-1b), Munc18-2 and Munc18-3 isoforms have also been identified (7–9). Munc18-2, also named Munc18b or muSec1 (mammalian ubiquitously Sec1), is the closest homologue of Munc18-1, showing 63% amino acid sequence identity (7).

The 67-kDa hydrophilic Munc18-1 protein has been shown to be necessary not only for vesicle exocytosis but also for docking of vesicles to the plasma membrane (10). Indeed, in the absence of Munc18-1 in neuronal cells, neither evoked nor spontaneous neurotransmission can operate (6). However, besides the reported positive effect of Munc18-1 in regulated exocytosis (6, 11–13), Munc18-1 has also been identified as a negative regulator of insulin secretion (14, 15). Still, Munc18-1 is primarily considered to be a neuronal protein, whereas the homologue Munc18-2 has a wider tissue expression profile. For instance, Munc18-2 is prominent in epithelial cells (16) and has been identified as a binding partner of Cab45, a Ca^{2+}-binding protein prominent in pancreatic acini (17). Recently Cab45/Munc18-2 was also detected in the endocrine β-cell (18). Munc18-2 exhibits the same syntaxin selectivity as Munc18-1 by binding syntaxin 1A, 2, and 3 (7, 16, 19). Worth mentioning is also that Munc18-2 has been shown to increase the secretory capacity of other mammalian cells, such as HeLa, HEK-293, and HT-1080 cells, and a mutation in the gene encoding Munc18-2 has been reported to impair cytotoxic granule exocytosis and

* This work was supported by The Swedish Research Council, The Novo Nordisk Foundation, The Swedish Council for Working Life and Social Research, The Stockholm County Council, Funds from Karolinska Institutet, Anders Otto Swärds/Ulrika Eklunds Foundations, the Family Erling-Persson Foundation, The Swedish Diabetes Association, The Berth von Kantzows Foundation, EuroDia, The Family Knut and Alice Wallenberg Foundation, VIBRANT (FP7-228933-2), Skandia Insurance Company Ltd., Strategic Research Program in Diabetes at Karolinska Institutet, Slovenian Research Agency Grant J3-7618-2334, and Max-Planck International Partner Group scheme.

[1] Both authors contributed equally to the work.

[2] To whom correspondence should be addressed: The Rolf Luft Research Center for Diabetes and Endocrinology, Karolinska Institutet, Karolinska University Hospital L1:03, SE-171 76 Stockholm, Sweden. E-mail: Per-Olof.Berggren@ki.se.

[3] The abbreviations used are: SNARE, soluble *N*-ethylmaleimide-sensitive factor attachment protein receptor; Cdk5, cyclin-dependent kinase 5; hGH, human growth hormone; HCRP, high Ca^{2+}-requiring pool; LCRP, low Ca^{2+}-requiring pool; AU, arbitrary units.

cause familial hemophagocytic lymphohistiocytosis type 5, FHL-5 (20, 21). Munc18-3 is expressed ubiquitously and has been demonstrated to be a functional partner of syntaxin 4 in the regulation of insulin-stimulated translocation of GLUT-4 in 3T3-L1 adipocytes (22), amylase release from parotid acinar cells (23), and in the second phase of insulin secretion (24, 25).

Phosphorylation of Munc18 proteins has been shown to affect exocytosis. Two kinases that have been identified to modify the function of Munc18-1 are cyclin-dependent kinase 5 (Cdk5) and protein kinase C (PKC) (26). Cdk5 is a small serine/threonine kinase that plays a pivotal role in many, in particular neuronal, processes by phosphorylating several different substrates (27, 28). Nevertheless, emerging evidence has demonstrated that Cdk5 is also vital in non-neuronal tissues, for example during muscle development, wound healing, and in insulin secretion from pancreatic β-cells (29–31). For its activation, Cdk5 is dependent upon association with one of the two regulatory subunits, p35 or p39 (32, 33). PKC, which is part of the diacylglycerol second messenger pathway, is a kinase that exists in many isoforms, of which several have an established regulatory role in distinct physiological steps of the exocytotic process (34). Despite the fact that endocrine β-cells share the same core exocytotic machinery as highly specialized neuronal synapses, regulated insulin secretion may require additional versatility. Primary β-cells have, in addition to the fastest phase of regulated exocytosis, slower phases of insulin secretion displaying different kinetics compared with the initial stimulated release (35, 36). In addition to maintaining a normal basal insulin secretion, the triggering threshold for stimulated insulin exocytosis and the magnitude of released hormone from β-cells need to be precisely tailored to different physiological conditions. To explore if the essential key regulator in synaptic transmission, Munc18-1, but also the closely related Munc18-2 protein contribute to the adaptability of insulin exocytosis from β-cells, we characterized their presence, abundance, and intracellular compartmentalization as well as their influence on Ca^{2+} sensitivity of the fastest phase of insulin secretion. We could demonstrate that both Munc18-1 and Munc18-2 affect insulin secretion, and depending on their phosphorylation status, they display distinct subcellular localization and control of Ca^{2+} sensitivity of exocytosis. We now suggest that in β-cells the fine-tuning of Ca^{2+} sensitivity of the exocytotic machinery partly relies on the presence of different Munc18 variants and their phosphorylation status, and these variations contribute to the versatility of regulated insulin release.

EXPERIMENTAL PROCEDURES

Antibodies—The following primary antibodies were used: a mouse anti-c-*Myc* antibody (9E10, Santa Cruz Biotechnology), a rabbit polyclonal anti-FLAG antibody (Sigma), and a mouse monoclonal anti-green fluorescent protein (GFP) antibody (JL-8, Clontech, BD Living Colors). Primary antibodies directed toward Munc18 variants were: a rabbit anti-Munc18-2 antibody (a kind gift from Dr. V. Olkkonen), a rabbit polyclonal anti-Munc18-1 (Synaptic Systems), and a mouse anti-Munc18-1 antibody (Transduction Laboratories). As a plasma membrane marker, a mouse monoclonal anti-Na^+/K^+ ATPase α-1 antibody (clone C464, Upstate Biotechnology) was used. Secondary antibodies were horseradish peroxidase-conjugated anti-rabbit and anti-mouse immunoglobulins (Rockland).

Reverse Transcriptase-Polymerase Chain Reaction (RT-PCR)—Total RNA was isolated from mouse brain (*ob*/*ob*), pancreatic islets (*ob*/*ob*) that contain 90–95%, β-cells (37), and the MIN6-m9 cell line using the GenElute™ Mammalian Total RNA kit (Sigma). RT-PCR was performed with the SuperScript™ III RT-PCR System (Invitrogen). RT-PCR were carried out using specific Munc18-1a, Munc18-1b, and Munc18-2 primers (Proligo, Sigma) designed according to GenBank™ sequences (accession numbers NM_001113569.1, NM_011503.4, and U21116.1). Primers were: Munc18-1a, 5′-tcgtccgcgtccttcagacac-3′ and 5′-tcagcgtgtccagcagtttc-3′; Munc18-1b, 5′-tcgtccgcgtccttcagacac-3′ and 5′-ctccattgttggagcctgatc-3′; Munc18-2, 5′-ccagcatgccaacgtgcag-3′ and 5′-cttgaggtcatcgaggaagc-3′. RT-PCR amplification was performed with the program 30 min at 55 °C, 2 min at 94 °C followed by 39 cycles of 94 °C for 1 min, 56 °C for 1 min, and 72 °C for 1 min, ending with 72 °C for 7 min. Amplification of syntaxin mRNA isoforms 1–3 was performed using the following primers: syntaxin 1A, 5′-atgaaggaccgaacccaggagc-3′ and 5′-tctatccaaagatgcccccga-3′; syntaxin 2, 5′-atgcgggaccggctgccgg-3′ and 5′-tcatttgccaaccgacaagcc-3′; syntaxin 3, 5′-atgaaggaccggctggagcat-3′ and 5′-ttatttcagcccaacggacaatg-3′. PCR products were separated by electrophoresis on 2% Tris acetate-EDTA-agarose gels and visualized by ethidium bromide staining, and 1-kb of DNA ladder (Invitrogen) was used as a size marker. PCR products were subjected to DNA sequencing (ABI Prism 377, Applied Biosystems), and the obtained results were verified by comparing with corresponding sequence entries in the National Centre for Biotechnology Information BLAST programs. All experiments were reproduced three times on separate RNA preparations.

Quantification of mRNA—Semiquantitative RT-PCR was performed with the primers for Munc18 and syntaxin isoforms described above and with glyceraldehyde-3-phosphate dehydrogenase (GAPDH) primers as the internal control. GAPDH primers were designed according to GenBank™ (accession numbers XM_147107 and X02231) to yield a PCR product of 208 bp: 5′-gacatcaagaaggtggtgaagc-3′ and 5′-gtccaccaccctgttgctgta-3′. A trace of [α-^{32}P]dCTP (3000 μCi/mmol, PerkinElmer Life Sciences) was included in the reactions, and the following program was used: 30 min at 55 °C and 2 min at 94 °C followed by 20 cycles of 94 °C for 1 min, 56 °C for 1 min, 72 °C for 1 min, and finally 72 °C for 7 min. Products were separated on 8% polyacrylamide Tris borate EDTA (TBE) and detected using phosphoimaging (BAS-1500, Fujifilm). Signal intensities were quantified by Image Gauge V3.45 (Fujifilm). Analyses were repeated at least three times on three separate RNA preparations, and the results are expressed as arbitrary units (AU). Statistical significance was evaluated using Student's unpaired *t* test.

Expression Vectors—Munc18-1 WT, a Munc18-1 PKC mutant (triple mutations from serine to alanine in PKC putative phosphorylation sites; Ser-306, -312, -313 → Ala), a Munc18-1 Cdk5 mutant (a mutation in Cdk5 phosphorylation site, Thr-574→ Ala-574), and Munc18-2 WT were cloned into the bicistronic expression vector pIRES2-EGFP (Clontech). The original constructs used for recloning were kind gifts from Drs. R. Toonen, M. Verhage, E. Stuenkel, and T. Südhof, respectively.

A construct encoding rat Munc18-2 WT, introduced in-frame into EGFP-C3 (Clontech), was kindly provided by Dr. U. Blank (19). A mutated rat Munc18-2 template (mutation in a potential Cdk5 phosphorylation site, Thr-573 → Ala 573) was created by PCR-directed mutagenesis and thereafter inserted into pIRES2-EGFP and also GFP tagged by cloning into a pEGFPC-1 vector (Clontech). FLAG- and myc-tagged Munc18-1 constructs were generated by PCR amplification of cDNA encoding the rat Munc18-1 WT sequence, and to achieve a more efficient translation initiation of the mRNAs, Kozak sequences were introduced. For generation of the YFP-Munc18-1 Cdk5 phosphorylation mutant, the mutation was introduced into Munc18-1 WT-YFP-C1 (Clontech) (a generous gift from Dr. Y. Liu). All construct were analyzed by DNA sequencing (ABI Prism 377, Applied Biosystems) and transfected into MIN6-m9, and expression was analyzed by immunoblotting. Pre-designed shRNA plasmids specifically generated to knock down the expression of Munc18-1 and Munc18-2 and co-expressing GFP were purchased from SuperArray, Bioscience Corp.

Isolation and Transfection of Primary β-Cells—Adult male NMRI mice were killed by cervical dislocation. Liberase (0.3 mg/ml, Roche Applied Science) dissolved in Hanks' buffered salt solution (Invitrogen) was injected into the pancreas through the bile duct. The pancreas was removed and digested for 10–15 min at 37 °C. Islets were collected by centrifugation and trypsinized into single cells. Cell culturing and transient transfections were performed as described previously (29).

Cell Culture, Gene Expression, and Western Blot in MIN6 Cells—Insulinoma MIN6-m9 cells were cultured, protein lysates were prepared, and immunoblotting was performed as described previously (29).

Subcellular Fractionation—MIN6-m9 cells transfected with tagged Munc18 templates were grown for 48 h in culture medium as described above. Before harvesting the cells for sucrose density gradient analysis, they were treated as follows: starvation for 1 h in Ca5 buffer (125 mM NaCl, 5.9 mM KCl, 1.28 mM $CaCl_2$, and 1.2 mM $MgCl_2$, 25 mM Hepes, and 0.1% bovine serum albumin (pH adjusted to 7.4 using NaOH)) and exposure to either stimulatory (DMEM, 25 mM glucose) or unstimulatory conditions (DMEM, 0.5 mM glucose) for 30 min followed by washing with PBS and trypsinization. Trypsinized cells were washed, homogenized, and centrifuged, and fractions were collected as described in Lilja *et al.* (29). 20 μg of protein from each fraction was analyzed by immunoblotting. For comparison and quantitative analysis of obtained signal of different tagged Munc18 proteins in different subcellular fractions, Image Gauge software was used. The results are expressed as percent protein found in plasma membrane fractions using Na^+/K^+ ATPase α-1 as a plasma membrane marker in unstimulated and stimulated MIN6 cells. All gradients were repeated three times, and Western blotting analyses were performed two times for gradient and construct and condition. After washing, membranes were incubated with horseradish peroxidase-conjugated immunoglobulins for 45 min at room temperature. Immunoreactive bands were detected by enhanced chemiluminescence (ECL plus or ECL Advance, Amersham Biosciences) using a CCD camera (LAS 1000, Fuji Photo Film Co., Ltd) that provides optimal linearity of signal intensity. The obtained quantification data were analyzed using unpaired Student's *t* test for significance evaluation.

Human GH Transfection and Secretion Assay—The culturing and transfection of INS-1E cells were performed as described previously (29).

Electrophysiology—Patch pipettes were pulled from borosilicate glass capillaries (GC150F-15, Harvard Apparatus Ltd) by a horizontal pipette puller (P-97, Sutter Instruments). The pipette resistance was 2–3 megaohms in cesium-based solution. The coverslip with cells was transferred from the incubator into the perfusion chamber and fixed with U-shaped platinum frame. 1.5 ml of extracellular solution consisting of 150 mM NaCl, 10 mM HEPES, 3 mM glucose, 5 mM KCl, 2 mM $CaCl_2$, 1 mM $MgCl_2$, pH 7.2, and osmolality of 300 ± 10 was added to the chamber. The pipette solution used for Ca^{2+}-induced capacitance measurement was composed of 5 mM NP-EGTA (Invitrogen), 4 mM $CaCl_2$, 0.1 mM Fura 6F (Invitrogen) together with 125 mM CsCl, 40 mM HEPES, 2 mM $MgCl_2$, 20 mM tetraethylammonium chloride, and 2 mM Na_2ATP with pH 7.2 and osmolality of 300 ± 10. All chemicals were purchased from Sigma unless otherwise indicated. Recordings were performed in the standard whole-cell mode via a patch clamp lock-in amplifier (SWAM IIc, Celica), low-pass-filtered, transferred to a PC via an A/D converter (National Instruments), and recorded on the hard disk using WinWCP V3.9.6 software (John Dampster, University of Strathclyde). The same software was used to apply voltage protocol for identifying β-cells by their Na^+ current inactivation pattern. A continuous sine voltage was applied to measure resting membrane capacitance (C_m), a parameter that is proportional to membrane surface area. Signal processing was done using Matview (Wise Technologies, Ljubljana, Slovenia) and Matlab (Mathworks). The number of cells investigated varied between 5 and 20, and the data were evaluated using one-way analysis of variance and Student's *t* test.

Ca^{2+} Measurements—Fura 6F (Molecular Probes, 0.1 mM in pipette solution) was used to measure intracellular Ca^{2+} concentrations ($[Ca^{2+}]_i$) simultaneously with the patch clamp recordings. Fura 6F was excited at 380 nm with a monochromator (Polychrome IV; TILL Photonics). Long pass dichroic mirror reflected the monochromatic light above 400 nm from the perfusion chamber and transmitted the emitted fluorescence, which was further filtered through a 420-nm barrier filter. The fluorescence intensity was measured with photodiode (TILL Photonics). $[Ca^{2+}]_i$ was calculated as described previously (38).

RESULTS

Expression and Abundance of Different Munc18 and Syntaxin Isoforms in Pancreatic β-Cells—It has previously been shown that Munc18-1, the "neuronal" Munc18 protein, is present in pancreatic β-cells, but if both splice variants are expressed is not known (14). Munc18-2 has been considered to be the more or less universally expressed isoform, being expressed in, for example, insulinoma cell lines and primary β-cells (8, 18). However, a valid study of Munc18 expression levels and splice variants has not yet been performed due to the fact that antibodies directed toward either Munc18-1 or

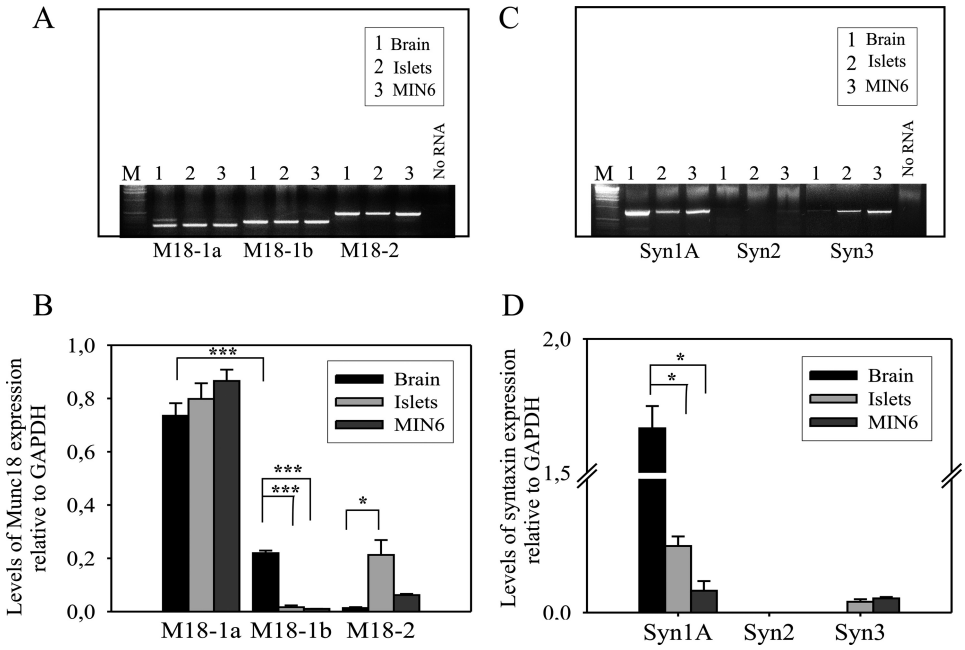

FIGURE 1. **Expression of Munc18 and syntaxin mRNA isoforms in brain, islets, and MIN6 cells.** *A*, RT-PCR was performed on total RNA with Munc18-1a, Munc18-1b, and Munc18-2 specific primers. The length of each amplified fragment was consistent with the expected lengths, estimated from the nucleotide sequences of the different Munc18 isoforms (236, 302 and 472 bp, respectively). *M* = 1kb DNA ladder. *B*, semiquantitative RT-PCR of Munc18-1a, Munc18-1b and Munc18-2 mRNAs was performed using GAPDH as internal control. *C*, syntaxin 1A, 2, and 3 mRNAs were detected with RT-PCR in brain, islets, and MIN6 cells. Sizes of amplified products were 868, 873, and 870 bp, respectively. *D*, semiquantitative RT-PCR identified syntaxin 1A in brain, pancreatic islets, and MIN6 cells. The level of syntaxin 2 was too low to be quantified, and syntaxin 3 was only detected in islets and MIN6 cells. All experiments were performed three times on three separate RNA preparations, and statistical analysis was performed using unpaired Student's *t* test. *, $p < 0.05$; ***, $p < 0.001$.

Munc18-2 usually demonstrate a significant cross-reactivity. Expression of Munc18-1/2, therefore, needs to be analyzed at the mRNA level. To address this, we designed isoform specific PCR primer pairs to analyze the expression pattern of the two Munc18-1 splice variants, the Munc18-2 mRNA as well as their corresponding syntaxin partners. RT-PCR analyses were performed on RNA isolated from *ob*/*ob* mouse islets (containing 90–95% β-cells) and mouse insulinoma MIN6 cells and are compared with the expression found in *ob*/*ob* mouse brain. The results demonstrated the presence of two splice variants of Munc18-1, Munc18-1a and Munc18-1b, and also Munc18-2 mRNA both in primary β-cells and in the insulin secreting MIN6 cell line (Fig. 1*A*). An additional PCR product was obtained in Munc18-1a amplification from brain mRNA. However, as DNA sequence analyses showed that the PCR product corresponded to both Munc18-1a and Munc18-1b sequences, it was viewed as an artifact. Semiquantitative analyses of mRNA transcripts of the different protein variants were performed to determine expression levels using GAPDH as an internal standard (Fig. 1*B*). Relative quantification showed that Munc18-1a mRNA was the most abundant isoform and expressed at similar levels in mouse brain, mouse islets, and MIN6 cells (0.74, 0.80, and 0.87 arbitrary units (AU), respectively). In comparison, the level of Munc18-1b was low in brain (0.22 AU; ***, $p < 0.001$) and just detectable in mouse islets and MIN6 cells (0.02 and 0.01 AU, respectively; ***, $p < 0.001$). Munc18-2 mRNA was most abundant in islets and expressed at low levels in brain and MIN6 cells (0.21, 0.01, and 0.02 AU, respectively; *, $p < 0.05$) (Fig. 1*B*). RT-PCR performed with syntaxin isoform-specific primers on brain and β-cell mRNA detected syntaxin 1A, 2, and 3 in our samples. With semiquantitative RT-PCR (Fig. 1*D*) syntaxin 1A expression was found to be prominent in brain, lower in islets, and barely detectable in MIN6 cells (1.67, 0.15, and 0.05 AU, respectively; *, $p < 0.05$). Syntaxin 3 was not detected in brain but was present at low levels in islets and MIN6 cells (Fig. 1*D*). Although syntaxin 2 was also detected with RT-PCR (Fig. 1*C*), the levels were too low to produce quantifiable signals in any of the tissues analyzed by semiquantitative RT-PCR (Fig. 1*D*). Taken together, the mRNA expression of Munc18 and syntaxin isoforms differs in islets, brain, and in the immortalized insulin-secreting MIN6 cell line. Consistently, Munc18-1a was the major Munc18 isoform expressed. However, the expression of Munc18-2 mRNA was surprisingly high in primary β-cells compared with brain and MIN6 cells.

Subcellular Distribution of WT and Phosphorylation Mutants of Munc18 Proteins Differs in Unstimulated and Stimulated MIN6 Cells—β-Cells are glucose sensors that upon increased glucose metabolism close their K_{ATP} channels, resulting in depolarization of the cell. Depolarization opens voltage-gated Ca^{2+} channels, and the concomitant Ca^{2+} influx triggers insulin secretion. To investigate and compare the subcellular localization of Munc18-1 and Munc18-2 WT proteins plus the corresponding phosphorylation mutants during resting and stimulatory conditions, we used the insulin-secreting cell line MIN6. This cell line was used to obtain enough transiently transfected cells for sucrose gradient analyses. Quantitative analyses of relative levels of different Munc18 proteins localizing to plasma membrane fractions (peaking in fractions ~5–9) were performed using endogenously expressed Na^+/K^+ ATPase as the plasma membrane marker. The results were displayed as the percent of Munc18 protein associated with the plasma membrane compared with maximal signal. Analyses

demonstrated that the majority of the Munc18-1 WT protein was present in soluble fractions in resting MIN6 cells (0.5 mM glucose) with a limited protein pool, 37.4%, associated with plasma membrane (Fig. 2, *A*, *B* (*left panel*), and *C*). Interestingly, the localization of the phosphorylation mutants of Munc18-1 revealed a different localization compared with the WT protein. In unstimulated cells, Cdk5 and PKC phosphorylation mutants were enriched in the plasma membrane fractions. As

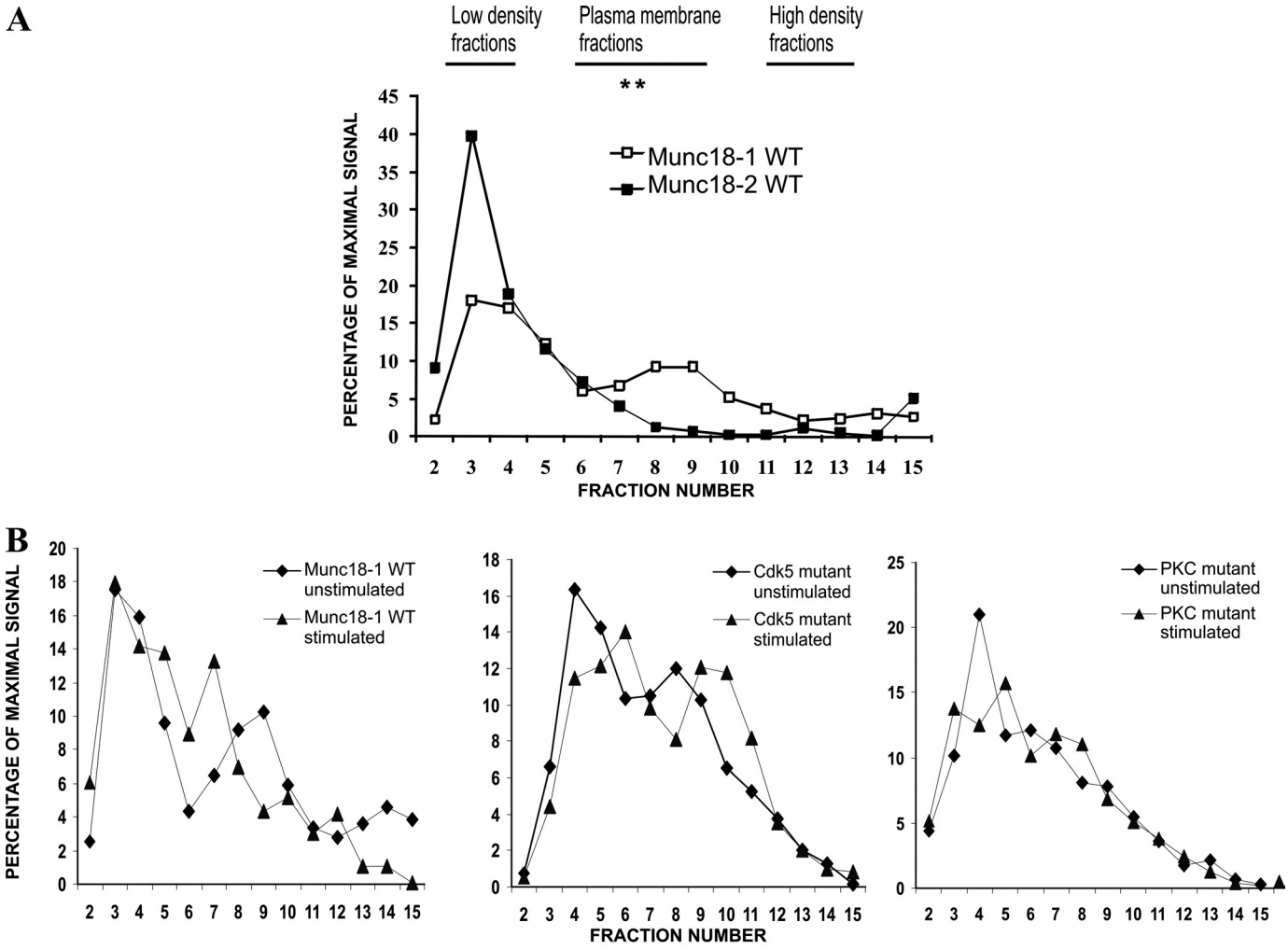

C

	Munc18-1 WT	Cdk5 mutant	PKC mutant
Unstimulated	37,4 ± 2,2 %	63,0 ± 6,07 % *	54,6 ± 3,7 % *
Stimulated	66,0 ± 3,7 % **	65,6 ± 7,3 %	62,4 ± 4,9 %

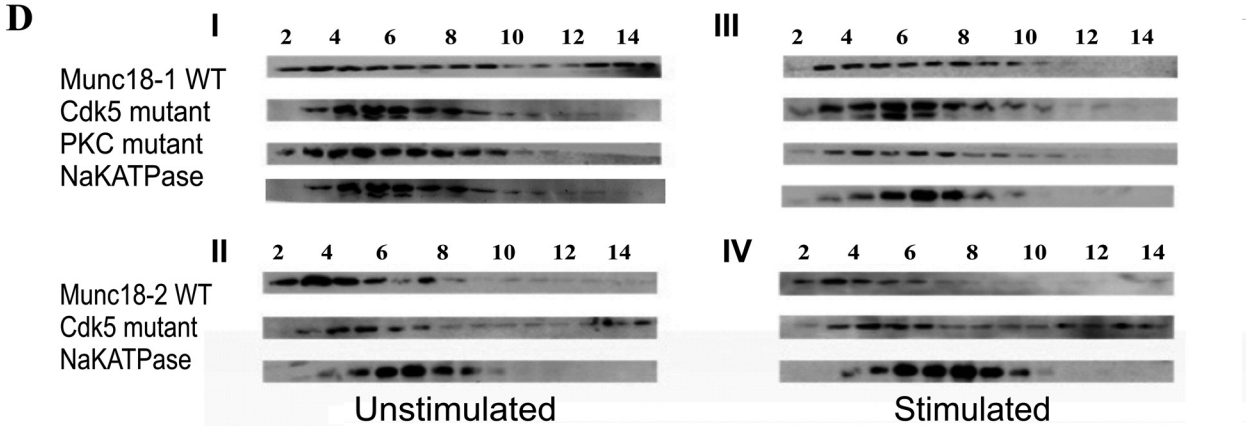

much as 63.0 and 54.6%, respectively, of the total detected protein colocalized with the Na^+/K^+ ATPase marker (Fig. 2, *B*, *middle* and *right panel*, and *C*; *, $p < 0.05$). When MIN6 cells were stimulated with 25 mM glucose, there was a quantitative recruitment of Munc18-1 WT to the plasma membrane fractions, demonstrated as an increase of percentage membrane bound protein (66.0%, Fig. 2*C*, **, $p < 0.01$). On the other hand, glucose stimulation of MIN6 cells did not noticeably increase or decrease the amount of already membrane associated Munc18-1 PKC and Cdk5 phosphorylation mutants (65.6 and 62.4%, respectively) (Fig. 2, *B*, *middle* and *right panel*, *C*, and *D*, *I* and *III*). We also compared the difference in subcellular localization between Munc18-1 WT and Munc18-2 WT proteins. During unstimulated conditions, the Munc18-2 WT protein was predominantly found in low density fractions corresponding to a cytoplasmic localization (Fig. 2, *A* and *D*, *II*). The amount of Munc18-2 protein in the plasma membrane fractions was relatively small compared with what we observed for the Munc18-1 WT protein (24.8% compared with 37.4%, respectively; **, $p < 0.01$). However, when analyzing subcellular distribution of the Cdk5 phosphorylation mutant of Munc18-2 in unstimulated cells, a small difference in the subcellular localization compared with overexpressed WT protein was observed. An apparent peak of mutant Munc18-2 protein was present in fractions 4 and 5, where for example trans-Golgi network can be found, whereas the WT protein peaked in fraction 3, corresponding to cytoplasmic fractions containing mainly small membranous organelles and soluble proteins (Fig. 2*D*, *II*). No significant translocation changes analogous with those found for the Munc18-1 WT protein and relative to the Na^+/K^+ ATPase marker in response to glucose stimulation were observed for Munc18-2 WT. Amounts of the Munc18-2 protein co-localizing with plasma membrane fractions were similar, 24.8 and 26.7%, for unstimulated and glucose-stimulated conditions, respectively ($p = 0.44$). The absence of the Cdk5 phosphorylation site in the Munc18-2 template (Munc18-2 Cdk5 phosphorylation mutant) did not seem to considerably affect subcellular distribution of Munc18-2 protein after glucose stimulation ($p = 0.49$; Fig. 2*D*, *II* and *IV*). In conclusion, Munc18-1 WT demonstrates a glucose-dependent translocation in MIN6 cells, whereas the PKC and Cdk5 phosphorylation mutants of Munc18-1 are sequestered in the plasma membrane already at resting conditions. Munc18-2 is, phosphorylated or not, mainly localized to cytosolic fractions irrespective of stimulation status.

Munc18-1 and Munc18-2 Positively Affect Glucose-stimulated Hormone Secretion—Glucose stimulation of β-cells triggers, via a series of intracellular metabolic processes, insulin release. The Munc18-1 protein demonstrated a glucose-dependent subcellular translocation, whereas the Munc18-2 protein did not. To investigate if the different Munc18 proteins had an effect on glucose-stimulated secretion, we took advantage of the human growth hormone (hGH) assay employed in INS-1E cells. We cotransfected cells with a vector expressing hGH and constructs encoding Munc18-1 WT, Munc18-2 WT, or control (pIRES2-EGFP, mock) followed by examination of the secretory response. By increasing glucose concentrations from 3 to 10 mM in mock-transfected cells, a significant increase, 249 ± 7%, of secretion was observed (***, $p < 0.001$; Fig. 3). This corresponds to 16.2 ± 1.1% of total hGH (Fig. 3; *Mock*). The percentage of released hGH at 10 mM glucose was further enhanced by overexpressing either the Munc18-1 WT or the Munc18-2 WT protein. Compared with control cells, Munc18-1 and Munc18-2 overexpression augmented the secretory response at elevated glucose concentration with 122 ± 6 and 123 ± 5%, respectively. This is consistent with 19.7 ± 1.2% (Munc18-1) and 19.8 ± 0.9% (Munc18-2) of total hGH secreted. These effects were statistically significant (*, $p < 0.05$). At basal conditions (3 mM glucose), there was no significant differences between control or Munc18-transfected cells. Thus, we could conclude that both Munc18-1 and Munc18-2 confer an overall positive effect on glucose-stimulated secretion. This was shown with the hGH release assay, a method that measures hormone release during 30 min of stimulation, thus reflecting both faster and slower phases of glucose-stimulated secretion.

Membrane Capacitance Measurements and Slow Photorelease—Physiological activation of β-cells is through depolarization-induced opening of voltage-gated Ca^{2+} channels. As we and others previously reported, significant reduction of the functional density of channels during cell isolation procedures can contribute to an unknown source of variability (39). Therefore, we decided to use slow photorelease to increase the overall Ca^{2+} concentration in the β-cell to stimulate regulated exocytosis and to specifically examine the Ca^{2+} sensitivity of the fastest phase of insulin release (40). Single β-cells were patch pipette-loaded with Ca^{2+} caged to NP-EGTA buffer and, after buffer equilibration in the cytosol, subjected to slow photorelease to increase the cytosolic free Ca^{2+} concentration ($[Ca^{2+}]_i$)

FIGURE 2. **Munc18-1 and Munc18-2 proteins distribute differently in sucrose gradient analyses in insulin-secreting MIN6 cells.** *A*, homogenates from unstimulated MIN6 cells transfected with tagged Munc18-1 WT or Munc18-2 WT were fractionated by sucrose density gradient fractionation. Quantification of Munc18-1 (*open squares*) and Munc18-2 (*filled squares*) using anti-Na^+/K^+ ATPase-1 antibody as a plasma membrane marker was performed and is presented as the average percent of maximal signal. The Munc18-2 WT protein was almost exclusively enriched in soluble fractions, whereas the Munc18-1 WT isoform demonstrated a more widespread distribution. The amount of the two Munc18 isoforms in the plasma membrane fractions (~5–9) was significantly different (**, $p < 0.01$). *B*, fractionation and subcellular localization of Munc18-1 WT and Munc18-1 proteins mutated in PKC and Cdk5 phosphorylation sites in unstimulated and glucose-stimulated MIN6 cells is shown. Munc18-1 WT and phosphorylation mutants associated differently with the plasma membrane (fractions ~5–9) in unstimulated MIN6 cells (0.5 mM), with mutants preferentially enriched in the plasma membrane (*, $p < 0.05$). The Munc18-1 WT protein was recruited to the plasma membrane upon glucose stimulation (25 mM) of MIN6 cells, whereas the mutated proteins remained sequestered in the plasma membrane fractions (~5–9). *C*, a table shows the mean values of the quantified amounts of the Munc18-1 WT protein and Munc18-1 phosphorylation mutant proteins in plasma membrane fractions during unstimulated and glucose-stimulated conditions. *D*, representative immunoblots of different Munc18 templates in unstimulated and glucose-stimulated MIN6 cells are shown. Fractions 2–15 of whole cell homogenates were resolved on SDS gels, and proteins were detected with the appropriate antibodies. The distribution of Munc18 WT proteins and kinase phosphorylation mutants in unstimulated MIN6 cells was compared with potential localization changes during stimulatory conditions. All fractionation studies for each construct and each condition were performed at least three times. Data were analyzed using Student's unpaired *t* test, and *$p < 0.05$ was considered statistically significant.

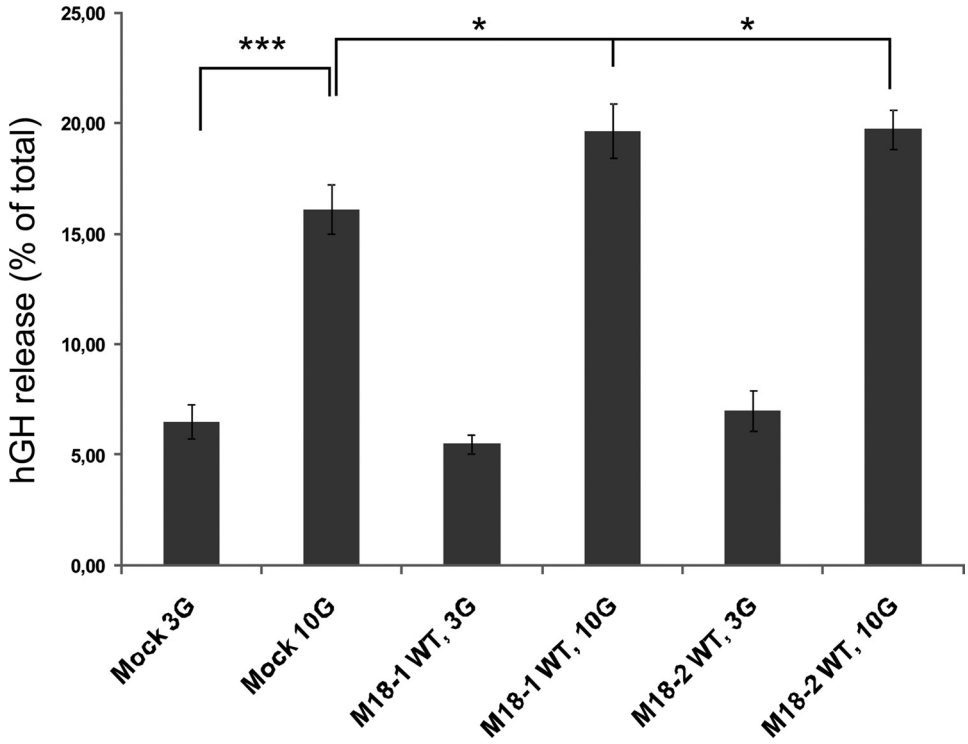

FIGURE 3. **Munc18-1 and Munc18-2 as positive effectors in glucose-stimulated hGH secretion in INS-1E cells.** INS-1E cells were transfected with Munc18-1 WT, Munc18-2 WT, Munc18-2 Cdk5 phosphorylation mutant, or pIRES2-EGFP vectors (control) in combination with a hGH expression construct. Glucose-stimulated secretion was triggered by incubation of INS-1E cells at 3 or 10 mM glucose for 30 min. Secreted hGH is presented as the percent of total hGH. The average percent of total hGH released is calculated in at least three experiments (each run in duplicates). Data were analyzed by Dunnett's test and are presented as the mean ± S.E. *, $p < 0.05$; ***, $p < 0.001$.

to the range of a few μM (Fig. 4*A*). The single β-cell exocytotic activity was assessed as a change in membrane capacitance (C_m), a parameter proportional to the plasma membrane surface area using high resolution whole-cell patch clamp recordings (Fig. 4*B*). The slow photorelease produced a fast ramp-like increase in $[Ca^{2+}]_i$ that peaked after about 5 s and reached the maximal amplitude after about 10 s (Fig. 4*A*). The kinetics of the induced Ca^{2+} change closely resembled the kinetics of a Ca^{2+} change produced by activation of voltage-gated Ca^{2+} channels using depolarization trains (39). The ramp-like increase in $[Ca^{2+}]_i$ typically resulted in two kinetic phases of membrane expansion with maximal amplitudes designated amp1 and amp2 for the first and the second component of fast exocytosis, respectively (Fig. 4*B*). The time derivatives of the C_m traces showed two separated processes. The maximal rates of C_m change within each phase have been accordingly termed rate1 and rate2 (Fig. 4*C*). To assess the Ca^{2+} dependence of the overall exocytotic process, we first plotted the parameters we could measure at steady state $[Ca^{2+}]_i$ (typically after more than 5 s of slow photorelease) against the peak $[Ca^{2+}]_i$ (Ca_{peak}; Fig. 4, *E* and *F*). Both amp2 and rate2 showed clear Ca^{2+} dependence in mock-transfected β-cells, but the data were substantially scattered (Fig. 4, *E* and *F*). However, detailed analysis of the experimental traces revealed that the initial threshold level for $[Ca^{2+}]_i$ (Ca_{tr}) to trigger the C_m increase (2.2 ± 0.4 μM, $n = 28$) was reproducible (Fig. 4*D*). Moreover, we found that the Ca^{2+} dependence followed the Hill saturation kinetics with high cooperativity. The half-maximal rate of the C_m change was achieved at 2.4 ± 0.4 μM $[Ca^{2+}]_i$, $n = 28$, (EC_{50}; Fig. 4*D*, *inset*). The maximal rate1 of the C_m changes in mock-transfected β-cells peaked between 100 and 700 femtofarads/s. The measured maximal rate1 in control (not transfected) and mock-transfected β-cells was comparable with the maximal rate achieved in control β-cells in tissue slices that were stimulated with brief depolarization pulses (41).

Overexpression of Munc18-1 and Munc18-2 WT Isoforms Shifts Ca^{2+} Sensitivity of Exocytotic Activity—In neuronal cells Munc18-1 function has been thoroughly investigated, and this protein is indispensible for synaptic transmission. Munc18-1 has been identified to operate in at least three different configurations, associating with the SNARE proteins at steps immediately upstream of or at membrane fusion. Whether this unique function of Munc18-1 in fast exocytosis also applies to endocrine cells remains to be investigated. To clarify a possible function of different Munc18 proteins in fast phases of insulin exocytosis, we transiently overexpressed different Munc18 variants in dispersed primary β-cells. Transient overexpression of Munc18-1 WT tended to shift Ca^{2+} dependence to lower Ca^{2+} sensitivity (2.6 ± 0.5 μM; Fig. 5*A*), *i.e.* higher $[Ca^{2+}]_i$ was required to trigger exocytosis compared with mock-transfected cells. On the other hand, overexpression of Munc18-2 WT shifted Ca^{2+} dependence to higher sensitivity (2.3 ± 0.5 μM; Fig. 5*A*). The difference in mean values of Ca_{50} of the two Munc18-transfected groups was greater than would be expected by chance ($n = 17–20$; *, $p < 0.05$). The amp1 and rate1 parameters were comparable in all tested groups (Fig. 5, *A* and *B*). Hence, this is the first indication that Munc18-1 and

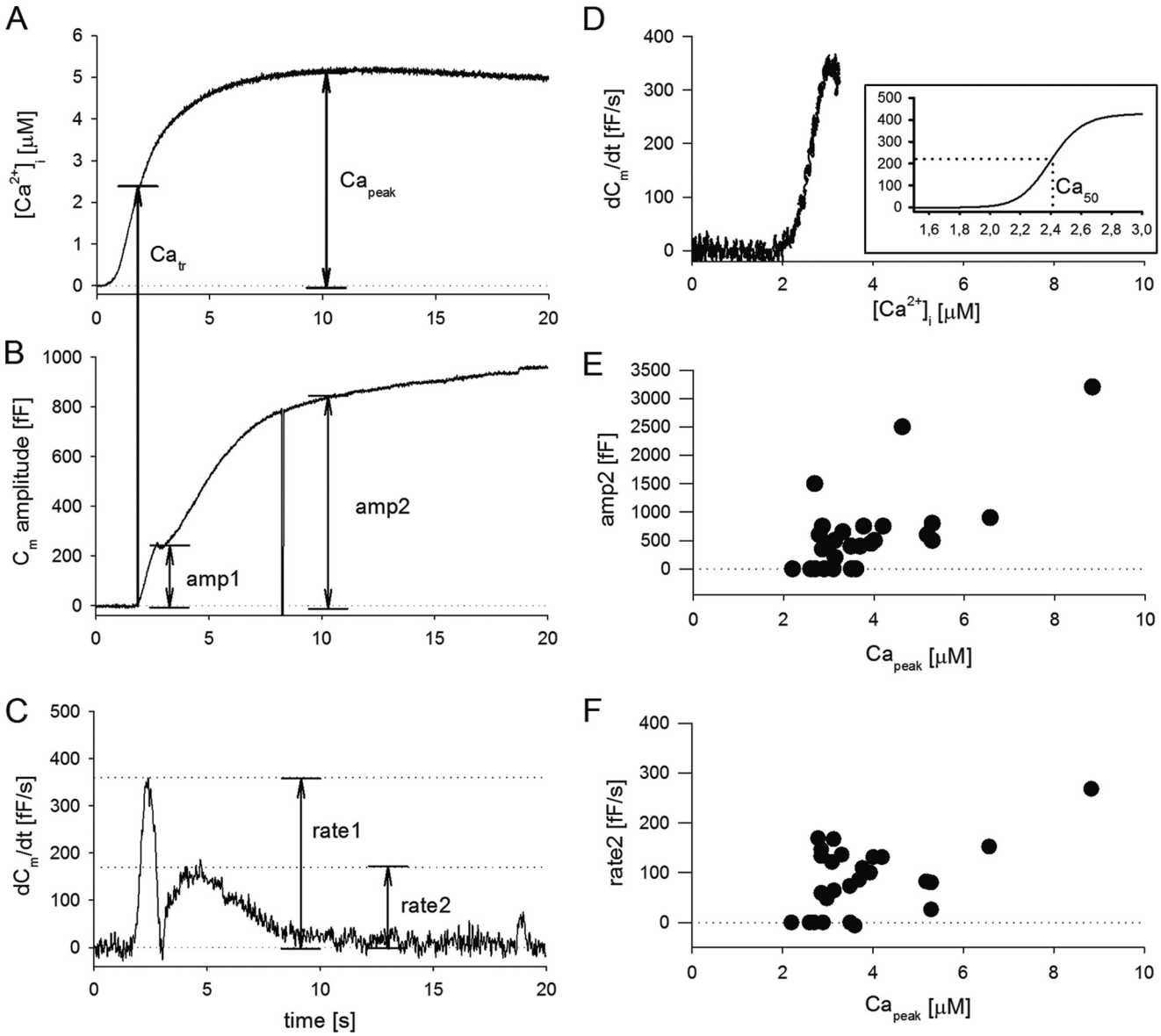

FIGURE 4. **Biphasic increase in C_m in primary β-cells transfected with pIRES2-EGFP (mock) and slow photorelease-induced increase in $[Ca^{2+}]_i$.** *A*, slow photorelease of Ca^{2+}-NP-EGTA produced a ramp-like increase in $[Ca^{2+}]_i$, reaching its peak amplitude (Ca_{peak}) after about 10 s. *B*, after reaching the threshold value of $[Ca^{2+}]_i$ (Ca_{tr}), a biphasic increase in C_m was triggered with the first phase reaching maximal amplitude within the first second after initiation (amp1) and second phase reaching maximal amplitude (amp2) at Ca_{peak}. *C*, shown is the time derivative of C_m amplitude presented in *B*, with the maximal rate of the first phase (rate1) and maximal rate of the C_m change during the second phase (rate2). *D*, the rate of C_m change (*D*) showed saturation kinetics when plotted *versus* $[Ca^{2+}]_i$, with high cooperativity and half-effective $[Ca^{2+}]_i$ (Ca_{50}) at 2.4 μM, $n = 28$. *Inset*, a curve shows the Hill function fit through the Ca^{2+} dependence data. *E*, shown is concentration dependence of the amp2 to Ca_{peak}. *F*, shown is concentration dependence of rate2 to Ca_{peak}. *fF*, femtofarad.

Munc18-2 may influence Ca^{2+} sensitivity of the secretory activity in endocrine cells differently.

Combined Overexpression of Munc18-1 and Munc18-2 WT Isoforms Significantly Increases the Total Amplitude of Fast Exocytosis in β-Cells—To further investigate a potential presence of parallel or integrative Munc18 protein functions in fast exocytosis in β-cells, we analyzed the second phase of the C_m change. For interpretation of the statistics, we compared the values for the cells where the peak $[Ca^{2+}]_i$ ranged between 3 and 5 μM for two reasons. First, in 95% of photorelease experiments, $[Ca^{2+}]_i$ demonstrated a saturated peak in this range (Fig. 5*C*), and second, we wanted to exclude the contamination from the first phase of fast exocytosis that occurs at lower $[Ca^{2+}]_i$. We observed that amp2 was significantly higher when either Munc18-2 WT was expressed alone or coexpressed with the Munc18-1 WT isoform (Fig. 5*D*; *, $p < 0.05$; **, $p < 0.01$). Rate2 did not change under any transfection conditions (Fig. 5*E*). The trend of reduced amp2 and rate2 in Munc18-1 WT overexpression is likely a result of shifted Ca^{2+} sensitivity. Unexpectedly, reduced expression levels of Munc18 proteins by introduction of knock-down templates did not significantly affect any of the measured parameters compared with control (SH C3) (Fig. 5, *B*, *D*, and *E*). A significant enlargement of amp2 was observed upon single overexpression of Munc18-2 WT, mirroring an increase in the number of exocytosed insulin granules during the second fast phase of exocytosis. An additional increase of amp2 was also obtained upon Munc18-1 and Munc18-2 coexpression, maybe indicating a potential

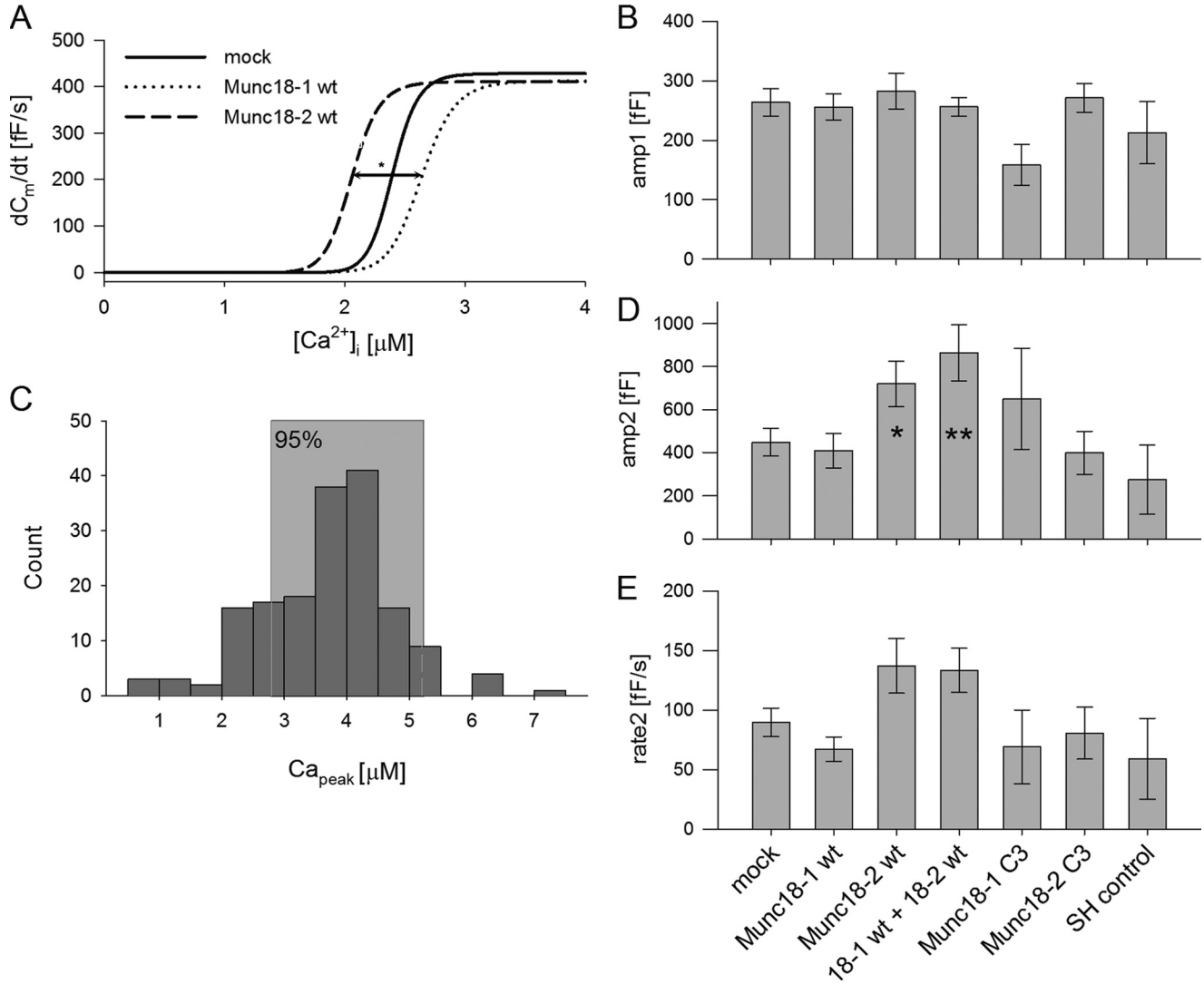

FIGURE 5. **Ca^{2+} dependence of C_m change in β-cells overexpressing different Munc18 WT isoforms.** *A*, shown are Hill function plots presenting Ca^{2+} dependence of the rate of the C_m change of the first phase of secretion in β-cells transiently transfected with mock, Munc18-1 WT, and Munc18-2 WT proteins. *B*, shown is a *bar chart* representation of amp1 in cells transfected with different WT isoforms and shRNA plasmids reducing the level of Munc18 proteins (as indicated in *E*). *C*, a histogram of the Ca_{peak} levels produced with photo-release shows that in 95% of all experiments $[Ca^{2+}]_i$ peaked between 3 and 5 μM. All statistics for the second phase were compared for this $[Ca^{2+}]_i$ range. *D*, shown is a *bar chart* representation of amp2. *E*, shown is a *bar chart* representation of rate2. The number of investigated cells was between 5 and 20. *, $p < 0.05$; **$p < 0.01$. *fF*, femtofarad.

additive effect of the two SM proteins (Sec1/Munc18) and suggesting the possibility of integrative secretory pathways.

Cdk5 and PKC Phosphorylation Mutants of Munc18 Isoforms and Ca^{2+} Sensitivity—Munc18 proteins are important hubs for protein phosphorylation. We tested the effect of two kinase systems by including Munc18-1 templates with a mutated Cdk5 phosphorylation site (P_{Cdk5} mutant, Thr-574 → Ala-574) or with all PKC phosphorylation sites altered (P_{PKC} mutant, Ser-306, -312, -313 → Ala) or Munc18-2 with a mutated Cdk5 phosphorylation site (Thr-573 → Ala-573). As shown in Fig. 6, *A* and *B*, the Ca^{2+} sensitivity of the first phase of the C_m change was significantly shifted when Munc18 isoform phosphorylation by the aforementioned kinases was impaired. Cells overexpressing Munc18-1 P_{Cdk5} tended to become less sensitive to $[Ca^{2+}]_i$ compared with mock-transfected control cells (Fig. 6*B*). On the other hand, Munc18-1 P_{PKC} and Munc18-2 P_{Cdk5} mutants had an opposite effect, significantly increasing the Ca^{2+} sensitivity of the process (Fig. 6*B*; ***, $p < 0.001$). This suggested that the phosphorylation events in these cases are important to prevent vesicle fusion before an adequate increase in $[Ca^{2+}]_i$ has been reached or before the action of corresponding phosphatases have facilitated the exocytotic process. In cotransfection experiments of Munc18-1 P_{Cdk5} and Munc18-2 P_{Cdk5}, the effect on the Ca^{2+} sensitivity resembled overexpression of Munc18-1 P_{Cdk5} alone, with the cells being significantly less sensitive to $[Ca^{2+}]_i$ (Fig. 6*B*; *, *$p < 0.01$). In fact, overexpression of Munc18-1 P_{Cdk5} has been dominant in all tested combinations. As for the second phase of the C_m change, amp2 was significantly elevated in the Munc18-1 P_{PKC}-overexpressing β-cells (Fig. 6*C*; **, $p < 0.01$). The absence of the phosphorylation event altered both rate1 and rate2 (Fig. 6, *A* and *D*). Significant reductions in rate2 were found after single transfections of Munc18-1 P_{Cdk5} and Munc18-2 P_{Cdk5} mutants but also after cotransfection of these two templates (Fig. 6*D*; **$p < 0.01$; *, $p < 0.05$). On the contrary, overexpression of the Munc18-1 P_{PKC} phosphorylation mutant significantly increased rate2 (Fig. 6*D*; *, $p <$

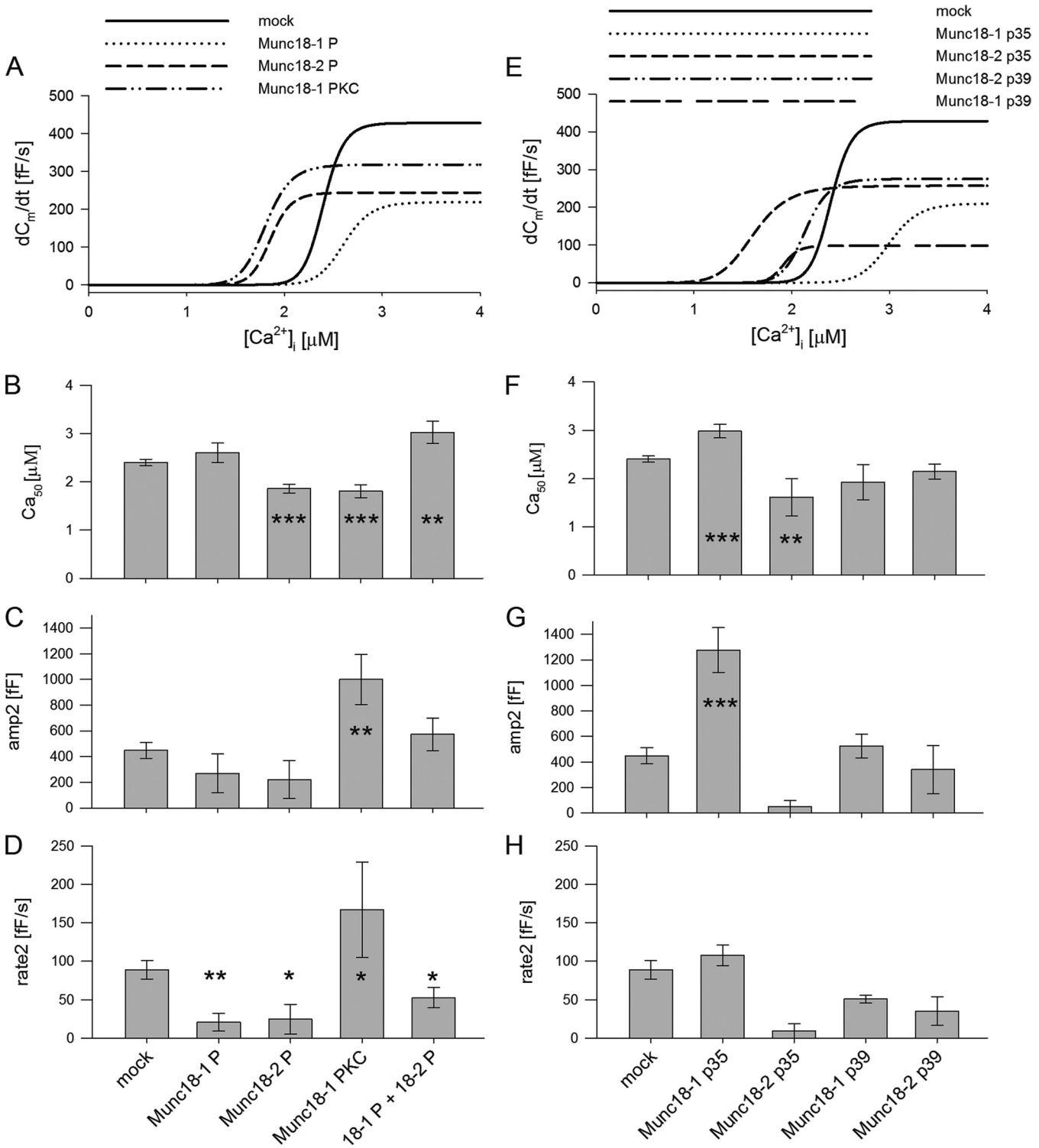

FIGURE 6. **Ca^{2+} dependence of the rate of C_m change in β-cells overexpressing Munc18 phosphorylation mutants or Ckd5 activators, p35 or p39.** *A*, shown are Hill function plots presenting Ca^{2+} dependence of the rate of C_m change of the first phase of fast exocytosis in β-cells transiently transfected with Mock, Munc18-1 P_{Cdk5} (*Munc18-1 P*), Munc18-1 P_{PKC}, and Munc18-2 P_{Cdk5} (*Munc18-2 P*) phosphorylation mutants. *B*, shown is a *bar chart* representation of the Ca_{50} in β-cells transfected with different phosphorylation mutants (as indicated in *D*). C, shown is a *bar chart* representation of amp2. *D*, shown is a *bar chart* representation of rate2. *E*, shown are Hill function plots presenting Ca^{2+} dependence of the rate of C_m change of first phase in β-cells transiently cotransfected with mock, Munc18-1 WT, or Munc18-2 WT and p35 or p39 Ckd5 activator constructs. *F*, shown is a *bar chart* representation of the Ca_{50} in β-cells transfected with different phosphorylation mutants (as indicated in *H*). *G*, shown is a *bar chart* representation of amp2. *H*, shown is a *bar chart* representation of rate2. The number of investigated cells was between 5 and 20. *, $p < 0.05$; **, $p < 0.01$, ***, $p < 0{,}001$. *fF*, femtofarad.

0.05). Briefly, phosphorylation of Munc18-1 and Munc18-2 proteins modulates both Ca^{2+} sensitivity and rate of insulin exocytosis. Any modification in the signaling pathway that would lead to a reduced Cdk5 phosphorylation of Munc18-1 should, therefore, require a stronger stimulation of β-cells to supply sufficient insulin to sustain glucose homeostasis within the organism.

Cotransfection of Cdk5 Activators and Munc18 WT Isoforms and Ca^{2+} Sensitivity—Next we addressed the role of the Cdk5 activators, p35 and p39, in the early process of fast insulin exocytosis induced by a ramp-like Ca^{2+} change. Overexpression of p35 or p39 constructs alone (not shown) or a combination of p39 with any Munc18 WT isoform had no effect on Ca^{2+} sensitivity (Fig. 6, *E* and *F*). We hypothesized that as we are only analyzing the effect within 10 s after increase of $[Ca^{2+}]_i$, maybe too few copies of natively expressed Munc18 proteins are accessible for phosphorylation by Cdk5 at the site of exocytosis, and consequently no significant augmentation was detected. However, considering the second phase of the fastest secretory response, combination of the p39 activator with either Munc18-1 WT or Munc18-2 WT tended to slightly but not significantly decrease rate2 (Fig. 6*H*). Cotransfections of either Munc18-1WT or Munc18-2 WT with the p35 Cdk5 activator resulted in significant shifts in Ca^{2+} sensitivity of the fast secretory component, as also seen in the change of EC_{50} value (Fig. 6, *E* and *F*; ***, $p < 0.001$; **, $p < 0.01$). In addition, combining Munc18-1 WT and p35 significantly enlarged amp2, *i.e.* the number of fusing vesicles (Fig. 6*G*; ***, $p < 0.001$), whereas p35 cotransfection with Munc18-2 WT almost completely abolished both amp2 and rate2. A delayed C_m response due to lower Ca^{2+} sensitivity of exocytosis when overexpression of p35 and Munc18-1 WT were combined could be the result of restrained granule fusion during the first phase of fast insulin exocytosis, which in turn leads to an accumulated number of vesicles released during the second kinetic phase, amp2. The lack of second phase release, represented by amp2 and rate2 parameters, in p35 and Munc18-2 WT double transfection could be attributed to the fact that this combination already facilitated vesicle fusion during amp1 at lower $[Ca^{2+}]_i$ and, thus, is not seen in the amp2 measurements. Despite the small effect of the p39 activator on maximal rate of secretory activity, both the rate and shift of Ca^{2+} sensitivity observed upon Munc18-1 WT single overexpression were normalized to control levels when the p39 activator and Munc18-1 WT protein were cotransfected. On the other hand, coexpression of Munc18 proteins with p35 disturbed the phosphorylation pattern and significantly changed Ca^{2+} sensitivity. Thus, these results indicate important roles for p35 and p39 Cdk5 activators in modulation of the kinetics of secretion by controlling the number and rate of releasable insulin granules but also in balancing Ca^{2+} sensitivity of the exocytotic process.

DISCUSSION

The pancreatic β-cell, in which the main function is to produce and secrete insulin, is a classic example of an endocrine cell. Nevertheless, β-cells express the full repertoire of SNARE and SNARE-regulating proteins found in neuronal cells, including the neuronal Munc18-1 protein. In addition, β-cells also express exocytotic proteins previously implicated in only non-neuronal exocytosis; for example, Munc18-2. We hypothesize that the presence of operators for several secretory pathways in β-cells might be one of the underlying reasons why this cell manages multiple phases of insulin secretion and demonstrates such a diversity and adaptability of the secretory response. This is an attribute important for the β-cell ability to tightly control glucose homeostasis in the body.

We first characterized the expression and abundance of endogenous Munc18 mRNAs and their corresponding syntaxin partners in islets, brain, and the insulinoma cell line MIN6. The results showed that the relative level of Munc18-2 was surprisingly high in islets from *ob*/*ob* mice, which on average contain 90–95% β-cells. The matching syntaxin isoforms 1 and 3 were also expressed.

Sec1/Munc18 proteins, originally identified as essential for membrane trafficking and secretion in yeast, are highly conserved among organisms. Null mutations of Munc18 homologue genes in a variety of species resulted in disruption or disturbances in regulated membrane fusion and/or specific intracellular trafficking pathways (42, 43). Particularly remarkable was the finding that targeted disruption of the mouse Munc18-1 gene produced a mutant that died shortly after birth (6). Even though brain development appeared normal, embryos from these mouse mutants were paralyzed due to the complete absence of both spontaneous and evoked synaptic transmission (6, 44). However, analyses in neuroendocrine chromaffin cells from Munc18-1 null embryos demonstrated a small but significant evoked secretion of catecholamines (45). This could indicate that some excitable cells possess both a Munc18-1-dependent secretory pathway and a yet redundant bypass route, allowing regulated exocytosis to occur in a Munc18-1-independent way.

Despite being the subject of intense studies, the precise regulatory roles and the sites of action of the Munc18-1 protein are not entirely elucidated. Several studies of Munc18-1 function in different organisms have demonstrated both negative and positive roles in regulated exocytosis (10). For example, in β-cells, the Munc18-1 protein has been proposed to have both inhibitory and positive effects on insulin release (14, 15, 29). Inconsistency in these results in β-cells could of course be a consequence of different experimental techniques measuring different phases of the insulin secretory cascade and thereby emphasizing different roles of the Munc18-1 protein. An additional possibility is that in some Munc18-1-expressing cells there also exists Munc18-1-independent secretory pathways. Besides binding monomeric syntaxin 1 in the closed conformation, recent findings show that Munc18-1 is capable of binding to the N-terminal part of syntaxin 1 in the open configuration (46). This direct interaction of Munc18-1 with the assembled SNARE complex promotes fusion and fusion pore kinetics (47). This positive effect contradicts the traditional theory of Munc18-1 playing an inhibitory role in secretion (46, 47). However, the negative effect on secretion is believed to be mediated through the formation of a high affinity syntaxin-1/Munc18-1 interaction, likely during vesicle docking, and thus preventing syntaxin-1 to assembly into the trimeric SNARE complex (46, 47). Transitions between the different binding modes of Munc18-1 are believed to be regulated by dynamic phosphorylation/dephosphorylation, and thereby kinase activity also partly contributes to the function ambiguity (48).

Munc18-1 and Munc18-2 can both bind the two target SNAREs syntaxin 1 and 3, which show 64% identity in amino acid structure and share conserved protein domains. Interest-

ingly, in HIT-T15 cells the plasma membrane protein syntaxin 3 has also been detected in the cytoplasm, functioning both as a modulator of insulin secretion and of Ca^{2+} channel activity (49). Munc18-2 has mostly been studied in epithelial tissues, where it controls apical regulated exocytosis, and in pancreatic acini, where it has been demonstrated to control Slp4a/granuphilin-syntaxin interactions and amylase secretion (17, 50). Coexpression of Munc18-1 and Munc18-2 has been confirmed in β-cells, somatotrophs in the anterior pituitary, mast cells, and PC12 cells (18, 52–54).

Phosphorylation of exocytotic proteins plays an important role in membrane trafficking and regulated secretion. We have previously shown that Munc18-1 is expressed in pancreatic β-cells and, together with Cdk5/p39, acts as a positive regulator of induced insulin exocytosis (29). The Cdk5 protein demonstrated a subcellular translocation from membrane-bound to cytosolic fractions when β-cells were stimulated by glucose (30). To investigate if WT or phosphorylation mutants of the Munc18 proteins changed localization as a response to cellular stimulation, we used transiently transfected MIN6 cells. Importantly, these experiments were performed using epitope-tagged Munc18 constructs, as Munc18 antibodies usually show a high degree of cross-reactivity between the different Munc18 isoforms. We observed a translocation of the Munc18-1 WT protein to plasma membrane fractions during glucose stimulation of β-cells, consistent with recent findings by Halban and coworkers (11). Interestingly, the absence of functional Cdk5 or PKC phosphorylation sites sequestered the Munc18-1 protein at the plasma membrane already under unstimulatory conditions, and these mutants remained membrane-bound also after stimulation. Obviously, both Cdk5 and PKC activity are required for the correct cycling of the Munc18-1 protein between the cytosolic- and membrane-bound state in β-cells. On the other hand, both Munc18-2 WT and its Cdk5 phosphorylation mutant remained cytosolic both in unstimulated and glucose-stimulated β-cells. Despite the difference in subcellular localization, both Munc18-1 and Munc18-2 were able to augment glucose-stimulated secretion. The increase in released hormone was modest but reproducible. It is possible to trigger additional signaling pathways and further enhance released hGH by adding a mixture of secretagogues (see for example Ref. 11), but we chose to look on only glucose-dependent secretion. In light of our findings it is of interest to compare with studies made in another cell type, namely the pituitary somatotrophs, where co-existence of Munc18-1 and Munc18-2 has also been observed (52). Anterior pituitary cells from Munc18-1 null mutants did not exhibit a complete absence of stimulated peptide secretion from large dense core vesicles. However, the large dense core vesicles appeared to reside at a larger distance from the membrane in mutants compared with WT cells when Munc18-1 was absent (52).

The Munc18-1 protein is involved in both early steps of the exocytotic cascade and in the events close to the actual membrane fusion. We investigated the fastest phase of regulated exocytosis by using the high resolution slow photorelease of caged Ca^{2+} and carefully evaluated the effects of Munc18 WT and phosphorylation mutated templates on the rate and amplitude of the first seconds of Ca^{2+}-triggered release in pancreatic β-cells. When Munc18-1 was overexpressed in β-cells, a higher $[Ca^{2+}]_i$ than in control cells was required to trigger secretion of release-competent vesicles. This may be explained by the fact that Munc18-1 together with syntaxin-1 forms a stable protein complex engaged in secretory granule docking, and higher intracellular Ca^{2+} levels are required for augmenting Munc18-1 transition and vesicle fusion with the plasma membrane. On the other hand, Munc18-2 overexpression shifted the Ca^{2+} sensitivity so that fusion of granules was also initiated at lower Ca^{2+} concentrations. This suggests that the different Munc18 proteins may support different granule populations that release their content at different $[Ca^{2+}]_i$. Indeed, the fastest phase of exocytosis could be divided further in two components demonstrating different fusion kinetics, rate1 and rate2, and with different amplitudes, amp1 and amp2. Both coexpression of Munc18-1 and Munc18-2 and single introduction of Munc18-2 further supported this by significantly increasing the number of releasable granules (amp2) exocytosed during the second secretory phase. This suggests that Munc18-2, in addition to assisting the release of the fastest phase of secretion (amp1), likely is important for refilling the granule pool released during amp2. Partial silencing of the Munc18-1 WT protein or the Munc18-2 protein (reduced to ~10–15%), quantified by Western blot, had no significant effect on the fastest phase of the exocytotic response. This suggests that the remaining endogenous protein is still sufficient to manage this phase of secretion. However, one should bear in mind that Munc18 is a regulatory protein involved in many steps preceding the fastest phase of regulated vesicle fusion, and a partial down-regulation of the expression level may not be the rate-limiting factor for the secretory step studied in our experimental set up. Munc18-1 Cdk5 phosphorylation mutant or Munc18-1 WT in combination with p35 lowered the Ca^{2+} sensitivity, *i.e.* increased the Ca^{2+} "threshold" for triggering of fusion. The non-phosphorylated form of the Munc18-1 protein is, similar to the WT template, still capable of stably docking the granules, which is followed by the shift to higher Ca^{2+} sensitivity, but the absence of Cdk5 phosphorylation leads to a negative effect on the rate and amplitude of exocytosis. On the other hand, adding p39 with Munc18-1 WT restored the Ca^{2+} sensitivity to the control levels compared with single overexpression of Munc18-1 WT, thus apparently increasing the release probability of this vesicle pool. This is similar to our earlier findings where Cdk5/p39 facilitated stimulated insulin secretion via Munc18-1, although the different experimental techniques used in the two different studies cannot be directly compared (29). This suggests that the rate-limiting step may be on the level of Munc18 phosphorylation, likely by p39-activated Cdk5. Overexpression of p39 activator alone tended to lower the maximal rate of membrane fusion in transfected β-cells but seemed to operate at a Ca^{2+} sensitivity comparable with that in control cells. On the contrary, overexpression of p35 activator produced an even more severe phenotype than Cdk5 mutants, suggesting a non-redundant and deactivating role for this subunit. All the different phosphorylation mutants of Munc18-1 and Munc18-2 negatively affected rate2 in the second phase of fast insulin exocytosis. Thus, different combinations of Munc18

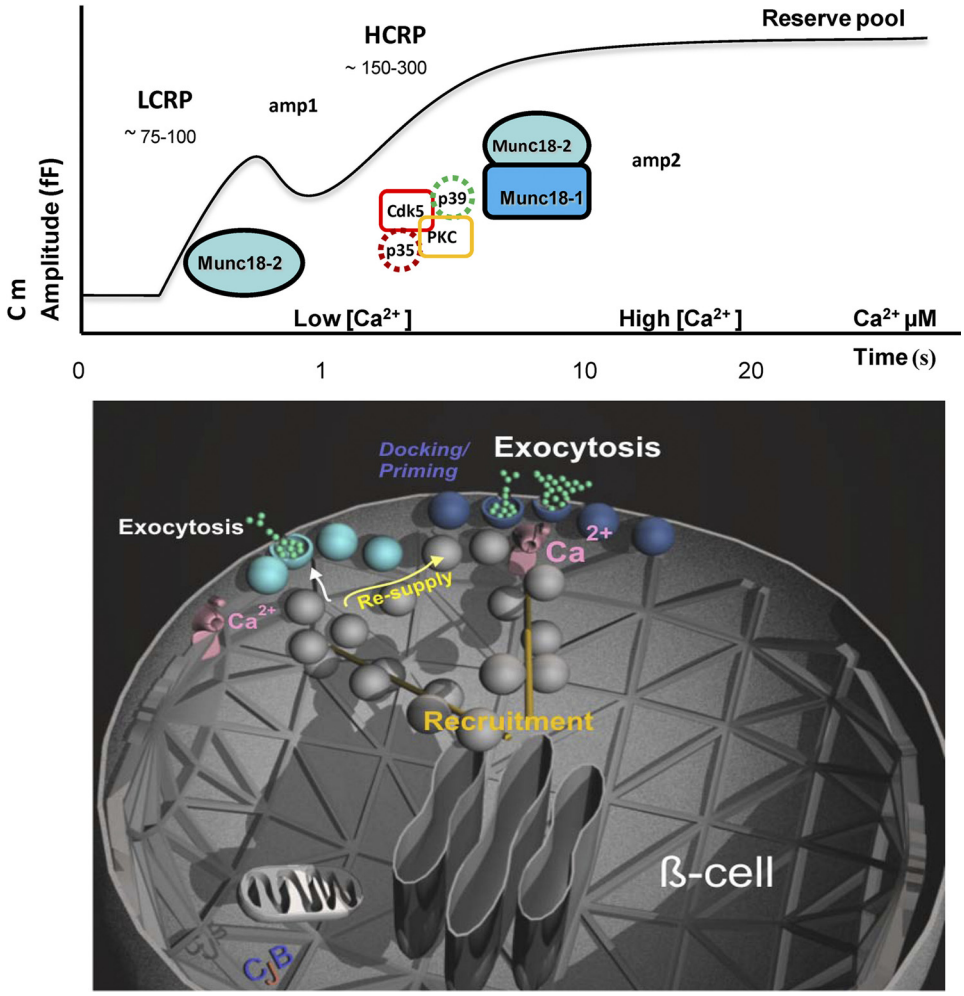

FIGURE 7. **Hypothetical model.** We propose a hypothetical model that illustrates the presence of two kinetic phases of fast insulin exocytosis. The model suggests that the existing releasable insulin granule population in β-cells is heterogeneous, with the simultaneous presence of vesicles requiring different $[Ca^{2+}]_i$ for fusion with the plasma membrane. The discrete difference of Ca^{2+} sensitivity for fusion of different granule pools coincides with different Munc18 proteins, and the role of the Munc18 proteins also depends on their phosphorylation state. Thus, Munc18-1 and Munc18-2 are associated differently with release of insulin through two parallel or integrative secretory pathways with different $[Ca^{2+}]_i$ sensitivity. Exocytosis of insulin is a multistep pathway. The conventional view is that vesicles are recruited to the plasma membrane where they are stably docked before going through a priming step that prepares them for fusion. Membrane vesicles, stably docked close to the plasma membrane (in *dark blue*) require high $[Ca^{2+}]_i$ to fuse and are expected to constitute a portion of the HCRP, released within 10 s post-stimulation (amp2, ~150–300 granules). Vesicles that exocytose at lower $[Ca^{2+}]_i$ (in *light blue*) are referred to as the LCRP, fuse within 1 s (corresponding to amp1 in the figure), probably represent a limited pool of vesicles, "possible newcomers," residing in the vicinity of the membrane and accompanied by the Munc18-2 protein. These vesicles may not proceed through the conventional Munc18-1-dependent docking step before fusion, thereby allowing a faster insulin response after stimuli. Likely, these LCRP vesicles also constitute a supply of granules to the conventional Munc18-1-dependent pathway where they will be stably docked, requiring a higher $[Ca^{2+}]_i$ for release (corresponding to amp2). Consequently, we suggest that the Munc18-2 protein has a dual function in insulin secretion; it assists a limited pool of LCRP vesicles in fast fusion at lower $[Ca^{2+}]_i$ to ensure an immediate insulin response and also supports refilling of the Munc18-1-dependent docked pool of insulin granules. Dr. Christopher J. Barker (*CJB*) helped with the illustration of this figure.

proteins and kinases modulate both the Ca^{2+} sensitivity and the rate of insulin exocytosis.

Conclusions and Hypothesis—Taken together, we now show that both Munc18-1 and Munc18-2 have the ability to augment glucose-stimulated secretion, and the Munc18-1 protein demonstrates a glucose-dependent cellular relocalization. We hypothesize that previous ambiguous results identifying Munc18-1 both as a positive and negative regulator of stimulated secretion in β-cells could depend on its role at different time points corresponding to different phases of insulin exocytosis. Thus, Munc18-1 could operate as a negative regulator during early, docking, or priming steps, but closer to the actual membrane fusion step, Munc18-1 mainly augments secretion. To investigate this possibility and to compare Munc18-1 and Munc18-2 function, we chose to analyze the fastest phase of regulated exocytosis in β-cells in more detail. Our examination of the initial fastest Ca^{2+}-triggered exocytosis demonstrates a release pattern with two kinetic phases and different Munc18 isoforms acting by modulating the Ca^{2+} sensitivity of releasable vesicles (Fig. 7). This suggests the existence of a heterogeneous population of release-competent granules in pancreatic β-cells, vesicles requiring high $[Ca^{2+}]_i$ for fusion, here referred as HCRP (high Ca^{2+}-requiring pool), and vesicles that fuse at lower $[Ca^{2+}]_i$, named LCRP (low Ca^{2+}-requiring pool) (see the *dark* and *light blue* vesicles in the hypothetical model in Fig. 7). The vesicles are presumably identical to what has previously been referred to as a highly Ca^{2+}-sensitive pool, present in β-cells (51, 55). HCRP are most likely located close to the

plasma membrane, associated, and managed by a Munc18-1-dependent secretory pathway. On the other hand, triggering of the LCRP fusion requires lower $[Ca^{2+}]_i$. Those vesicles are not necessarily directly attached to the plasma membrane, *i.e.* stably docked, and they appear to be more dependent on the cytosolic Munc18-2 protein. The rate and the amplitude of the release during the first seconds of the fastest insulin release also depend on the phosphorylation status of the different Munc18 proteins. Thus, whereas it seems that neuronal cells are completely dependent on a Munc18-1-operated secretory pathway, neuroendocrine tissues such as adrenal chromaffin cells and anterior pituitary cells have a limited capacity to perform Munc18-1-independent-regulated membrane fusion. The endocrine pancreatic β-cells appear to concurrently use several secretory pathways, whereas secretion mechanisms in the exocrine pancreas as well as the apical membrane fusion in epithelial cells completely rely on Munc18-1-independent pathways. The change in Ca^{2+} sensitivity, as reported in this paper, shows a dependence on different Munc18 homologous and presents a novel contribution to our understanding of the function of the β-cell. Moreover, it illustrates a new way of fine-tuning insulin release by different protein isoforms, which in addition can be phosphorylated to further increase the complexity. Further work will be needed to characterize the precise molecular mechanisms differentiating the Ca^{2+} sensitivity of insulin secretion. However, our finding that distinct Munc18 homologous play a role in this process is novel. In conclusion, we suggest that both Munc18-1 and Munc18-2 are important regulators of insulin secretion from pancreatic β-cells, and their collective function contributes to β-cells demonstrating such an adaptive secretory response to different physiological conditions and environmental cues.

Acknowledgments—We thank Drs. R. Toonen, M. Verhage, E. Stuenkel, and Y. Liu for Munc18-1 templates and Drs. T. Südhof, U. Blank, and V. Olkkonen for Munc18-2 constructs and antibody. We also thank Dr. Christopher J. Barker for kind help with the illustration in Fig. 7.

REFERENCES

1. Leibiger, I. B., Leibiger, B., and Berggren, P. O. (2008) *Annu. Rev. Nutr.* **28,** 233–251
2. Jacobsson, G., Bean, A. J., Scheller, R. H., Juntti-Berggren, L., Deeney, J. T., Berggren, P. O., and Meister, B. (1994) *Proc. Natl. Acad. Sci. U.S.A.* **91,** 12487–12491
3. Gauthier, B. R., and Wollheim, C. B. (2008) *Am. J. Physiol. Endocrinol. Metab.* **295,** E1279–E1286
4. Jahn, R., Lang, T., and Südhof, T. C. (2003) *Cell* **112,** 519–533
5. Südhof, T. C., and Rothman, J. E. (2009) *Science* **323,** 474–477
6. Verhage, M., Maia, A. S., Plomp, J. J., Brussaard, A. B., Heeroma, J. H., Vermeer, H., Toonen, R. F., Hammer, R. E., van den Berg, T. K., Missler, M., Geuze, H. J., and Südhof, T. C. (2000) *Science* **287,** 864–869
7. Hata, Y., and Südhof, T. C. (1995) *J. Biol. Chem.* **270,** 13022–13028
8. Katagiri, H., Terasaki, J., Murata, T., Ishihara, H., Ogihara, T., Inukai, K., Fukushima, Y., Anai, M., Kikuchi, M., and Miyazaki, J. (1995) *J. Biol. Chem.* **270,** 4963–4966
9. Halachmi, N., and Lev, Z. (1996) *J. Neurochem.* **66,** 889–897
10. Burgoyne, R. D., Barclay, J. W., Ciufo, L. F., Graham, M. E., Handley, M. T., and Morgan, A. (2009) *Ann. N.Y. Acad. Sci.* **1152,** 76–86
11. Tomas, A., Meda, P., Regazzi, R., Pessin, J. E., and Halban, P. A. (2008) *Traffic* **9,** 813–832
12. Fisher, R. J., Pevsner, J., and Burgoyne, R. D. (2001) *Science* **291,** 875–878
13. Schütz, D., Zilly, F., Lang, T., Jahn, R., and Bruns, D. (2005) *Eur. J. Neurosci.* **21,** 2419–2432
14. Zhang, W., Efanov, A., Yang, S. N., Fried, G., Kolare, S., Brown, H., Zaitsev, S., Berggren, P. O., and Meister, B. (2000) *J. Biol. Chem.* **275,** 41521–41527
15. Dong, Y., Wan, Q., Yang, X., Bai, L., and Xu, P. (2007) *Biochem. Biophys. Res. Commun.* **360,** 609–614
16. Riento, K., Jäntti, J., Jansson, S., Hielm, S., Lehtonen, E., Ehnholm, C., Keränen, S., and Olkkonen, V. M. (1996) *Eur. J. Biochem.* **239,** 638–646
17. Lam, P. P., Hyvärinen, K., Kauppi, M., Cosen-Binker, L., Laitinen, S., Keränen, S., Gaisano, H. Y., and Olkkonen, V. M. (2007) *Mol. Biol. Cell* **18,** 2473–2480
18. Zhang, Y., Kang, Y. H., Chang, N., Lam, P. P., Liu, Y., Olkkonen, V. M., and Gaisano, H. Y. (2009) *J. Biol. Chem.* **284,** 20840–20847
19. Martin-Verdeaux, S., Pombo, I., Iannascoli, B., Roa, M., Varin-Blank, N., Rivera, J., and Blank, U. (2003) *J. Cell Sci.* **116,** 325–334
20. Peng, R. W., Guetg, C., Tigges, M., and Fussenegger, M. (2010) *Metab. Eng.* **12,** 18–25
21. Côte, M., Ménager, M. M., Burgess, A., Mahlaoui, N., Picard, C., Schaffner, C., Al-Manjomi, F., Al-Harbi, M., Alangari, A., Le Deist, F., Gennery, A. R., Prince, N., Cariou, A., Nitschke, P., Blank, U., El-Ghazali, G., Ménasché, G., Latour, S., Fischer, A., and de Saint Basile, G. (2009) *J. Clin. Invest.* **119,** 3765–3773
22. Tellam, J. T., Macaulay, S. L., McIntosh, S., Hewish, D. R., Ward, C. W., and James, D. E. (1997) *J. Biol. Chem.* **272,** 6179–6186
23. Imai, A., Nashida, T., and Shimomura, H. (2004) *Arch. Biochem. Biophys.* **422,** 175–182
24. Jewell, J. L., Oh, E., and Thurmond, D. C. (2010) *Am. J. Physiol. Regul. Integr. Comp. Physiol.* **298,** 517–531
25. Oh, E., and Thurmond, D. C. (2009) *Diabetes* **58,** 1165–1174
26. Snyder, D. A., Kelly, M. L., and Woodbury, D. J. (2006) *Cell Biochem. Biophys.* **45,** 111–123
27. Dhavan, R., and Tsai, L. H. (2001) *Nat. Rev. Mol. Cell Biol.* **2,** 749–759
28. Lalioti, V., Pulido, D., and Sandoval, I. V. (2010) *Cell Cycle* **9,** 284–311
29. Lilja, L., Johansson, J. U., Gromada, J., Mandic, S. A., Fried, G., Berggren, P. O., and Bark, C. (2004) *J. Biol. Chem.* **279,** 29534–29541
30. Lilja, L., Yang, S. N., Webb, D. L., Juntti-Berggren, L., Berggren, P. O., and Bark, C. (2001) *J. Biol. Chem.* **276,** 34199–34205
31. Rosales, J. L., and Lee, K. Y. (2006) *BioEssays* **28,** 1023–1034
32. Ko, J., Humbert, S., Bronson, R. T., Takahashi, S., Kulkarni, A. B., Li, E., and Tsai, L. H. (2001) *J. Neurosci.* **21,** 6758–6771
33. Tang, D., and Wang, J. H. (1996) *Prog. Cell Cycle Res.* **2,** 205–216
34. Morgan, A., Burgoyne, R. D., Barclay, J. W., Craig, T. J., Prescott, G. R., Ciufo, L. F., Evans, G. J., and Graham, M. E. (2005) *Biochem. Soc. Trans.* **33,** 1341–1344
35. Henquin, J. C. (2009) *Diabetologia* **52,** 739–751
36. Jewell, J. L., Oh, E., and Thurmond, D. C. (2010) *Am. J. Physiol. Regul. Integr. Comp. Physiol.* **298,** R517–R531
37. Hellman, B. (1965) *Ann. N.Y. Acad. Sci.* **131,** 541–558
38. Sedej, S., Tsujimoto, T., Zorec, R., and Rupnik, M. (2004) *J. Physiol.* **555,** 769–782
39. Speier, S., and Rupnik, M. (2003) *Pflugers Arch.* **446,** 553–558
40. Skelin, M., and Rupnik, M. (2011) *Cell Calcium* **49,** 89–99
41. Rose, T., Efendic, S., and Rupnik, M. (2007) *J. Gen. Physiol.* **129,** 493–508
42. Toonen, R. F., and Verhage, M. (2003) *Trends Cell Biol.* **13,** 177–186
43. Novick, P., Field, C., and Schekman, R. (1980) *Cell* **21,** 205–215
44. Korteweg, N., Maia, A. S., Verhage, M., and Burbach, J. P. (2004) *Eur. J. Neurosci.* **19,** 2944–2952
45. Voets, T., Toonen, R. F., Brian, E. C., de Wit, H., Moser, T., Rettig, J., Südhof, T. C., Neher, E., and Verhage, M. (2001) *Neuron* **31,** 581–591
46. Rickman, C., Medine, C. N., Bergmann, A., and Duncan, R. R. (2007) *J. Biol. Chem.* **282,** 12097–12103
47. Dulubova, I., Khvotchev, M., Liu, S., Huryeva, I., Südhof, T. C., and Rizo, J. (2007) *Proc. Natl. Acad. Sci. U.S.A.* **104,** 2697–2702
48. Toonen, R. F., and Verhage, M. (2007) *Trends Neurosci.* **30,** 564–572
49. Kang, Y., Huang, X., Pasyk, E. A., Ji, J., Holz, G. G., Wheeler, M. B., Tsushima, R. G., and Gaisano, H. Y. (2002) *Diabetologia* **45,** 231–241

50. Fukuda, M., Imai, A., Nashida, T., and Shimomura, H. (2005) *J. Biol. Chem.* **280,** 39175–39184
51. Yang, Y., and Gillis, K. D. (2004) *J. Gen. Physiol.* **124,** 641–651
52. Korteweg, N., Maia, A. S., Thompson, B., Roubos, E. W., Burbach, J. P., and Verhage, M. (2005) *Biol. Cell* **97,** 445–455
53. Nigam, R., Sepulveda, J., Tuvim, M., Petrova, Y., Adachi, R., Dickey, B. F., and Agrawal, A. (2005) *Biochim. Biophys. Acta* **1728,** 77–83
54. Han, L., Jiang, T., Han, G. A., Malintan, N. T., Xie, L., Wang, L., Tse, F. W., Gaisano, H. Y., Collins, B. M., Meunier, F. A., and Sugita, S. (2009) *Mol. Biol. Cell* **20,** 4962–4975
55. Wan, Q. F., Dong, Y., Yang, H., Lou, X., Ding, J., and Xu, T. (2004) *J. Gen. Physiol.* **124,** 653–662